

Article

Vapor-Phase Fabrication of a Maleimide-Functionalized Poly-*p*-xylylene with a Three-Dimensional Structure

Shu-Man Hu ^{1,†}, Chin-Yun Lee ^{1,†} , Yu-Ming Chang ¹, Jia-Qi Xiao ¹, Tatsuya Kusanagi ¹, Ting-Ying Wu ¹, Nai-Yun Chang ¹, Jane Christy ¹, Ya-Ru Chiu ¹, Chao-Wei Huang ², Yen-Ching Yang ^{1,*}, Yu-Chih Chiang ^{3,4,*} and Hsien-Yeh Chen ^{1,4,5,*} 

¹ Department of Chemical Engineering, National Taiwan University, Taipei 10617, Taiwan; r09524083@ntu.edu.tw (S.-M.H.); r09524048@ntu.edu.tw (C.-Y.L.); r09524079@ntu.edu.tw (Y.-M.C.); r09524013@ntu.edu.tw (J.-Q.X.); r09524111@ntu.edu.tw (T.K.); tilee824@gmail.com (T.-Y.W.); Changnaiyun@ntu.edu.tw (N.-Y.C.); b07504085@ntu.edu.tw (J.C.); iwbs24921@gmail.com (Y.-R.C.)

² Department of Tropical Agriculture and International Cooperation, National Pingtung University of Science and Technology, Pingtung 912301, Taiwan; cw Huang@mail.npust.edu.tw

³ School of Dentistry, Graduate Institute of Clinical Dentistry, National Taiwan University and National Taiwan University Hospital, Taipei 10048, Taiwan

⁴ Molecular Imaging Center, National Taiwan University, Taipei 10617, Taiwan

⁵ Advanced Research Center for Green Materials Science and Technology, National Taiwan University, Taipei 10617, Taiwan

* Correspondence: youngeddie.tw@googlemail.com (Y.-C.Y.); munichiang@ntu.edu.tw (Y.-C.C.); hsychen@ntu.edu.tw (H.-Y.C.); Tel.: +886-2-33669476 (H.-Y.C.)

† Authors contributed equally to this work.



Citation: Hu, S.-M.; Lee, C.-Y.; Chang, Y.-M.; Xiao, J.-Q.; Kusanagi, T.; Wu, T.-Y.; Chang, N.-Y.; Christy, J.; Chiu, Y.-R.; Huang, C.-W.; et al. Vapor-Phase Fabrication of a Maleimide-Functionalized Poly-*p*-xylylene with a Three-Dimensional Structure. *Coatings* **2021**, *11*, 466. <https://doi.org/10.3390/coatings11040466>

Academic Editor: Alessandro Patelli

Received: 12 March 2021

Accepted: 13 April 2021

Published: 16 April 2021

Publisher's Note: MDPI stays neutral with regard to jurisdictional claims in published maps and institutional affiliations.



Copyright: © 2021 by the authors. Licensee MDPI, Basel, Switzerland. This article is an open access article distributed under the terms and conditions of the Creative Commons Attribution (CC BY) license (<https://creativecommons.org/licenses/by/4.0/>).

Abstract: A vapor-phase process, involving the sublimation of an ice substrate/template and the vapor deposition of a maleimide-functionalized poly-*p*-xylylene, has been reported to synthesize an advanced porous material, with readily clickable chemical interface properties, to perform a Michael-type addition of a maleimide functionality for conjugation with a thiol group. In contrast to the conventional chemical vapor deposition of poly-*p*-xylylenes on a solid surface that forms thin film coatings, the process reported herein additionally results in deposition on a dynamic and sublimating ice surface (template), rendering the construction of a three-dimensional, porous, maleimide-functionalized poly-*p*-xylylene. The process seamlessly exploits the refined chemical vapor deposition polymerization from maleimide-substituted [2,2]paracyclophane and ensures the preservation and transformation of the maleimide functionality to the final porous poly-*p*-xylylene products. The functionalization and production of a porous maleimide-functionalized poly-*p*-xylylene were completed in a single step, thus avoiding complicated steps or post-functionalization procedures that are commonly seen in conventional approaches to produce functional materials. More importantly, the equipped maleimide functionality provides a rapid and efficient route for click conjugation toward thiol-terminated molecules, and the reaction can be performed under mild conditions at room temperature in a water solution without the need for a catalyst, an initiator, or other energy sources. The introduced vapor-based process enables a straightforward synthesis approach to produce not only a pore-forming structure of a three-dimensional material, but also an in situ-derived maleimide functional group, to conduct a covalent click reaction with thiol-terminal molecules, which are abundant in biological environments. These advanced materials are expected to have a wide variety of new applications.

Keywords: vapor sublimation and deposition; functional poly-*p*-xylylene; maleimide; porous material; orthogonal conjugation

1. Introduction

Porous materials, owing to their remarkable interface properties, have been widely applied in sensing, catalysis, biomedical, drug delivery, adsorption/desorption applica-

tions, etc. [1–4]. These applications can especially be highlighted in their drug delivery and emerging biomedical applications due to the multiple premium interface properties that are required [5,6]. The benefits of porous structures are attributed to their large surface area, the adjustable number of pores, and a functionalized surface, which can provide multifunctional active sites [7]. In addition to porous properties, bioconjugation functionalities that provide selectivity and orthogonal reactivity, while avoiding any side reactions in the vast and diverse conditions of biological microenvironments, are key to achieving successful biointerface construction. For example, thiol–maleimide “click” chemistry and maleimide functional polymers selectively target thiol-containing cysteine residues in proteins and enzymes, with excellent levels of selective conjugation being achieved. Cysteine-reactive polymers can be applied to prevent the degradation of sensitive poly(ester) backbones [8]. In addition, the prototypical click chemistry reaction, Cu(I)-catalyzed azide–alkyne cycloaddition (CuAAC), involves a modification to the triazole-forming 1,3-dipolar cycloaddition. The application of CuAAC to produce fluorogenic compounds would be a powerful way to track biomolecules in the cell [9]. Specific reactions can also be applied for protein modification. The ligation between trans-cyclooctene and 3,6-di-(2-pyridyl)-s-tetrazine enables protein modification at low concentrations. This reaction can tolerate multiple functional groups and proceed in high-yield organic solvents, water, or cell media [10]. Recently, many bio-orthogonal reactions have been developed that enable the efficient formation of a specific product in complex environments, which is particularly beneficial for biological research [11].

These fascinating chemistries, however, have seldom been exploited during the fabrication of porous materials and are sporadically seen using complicated synthetic approaches [12] or by post-modification attempts, which involve using harsh solvents or potentially harmful chemicals during the modification process [13,14].

In the current study, we introduced a simple and versatile approach, based on a vapor-phase fabrication process, to produce a functionalized porous polymer material. Fabrication occurred by the vapor deposition of a poly-*p*-xylylene polymer on an iced substrate (vapor sublimation), which was discovered in our previous reports, and was compared to the conventional vapor deposition of poly-*p*-xylylene on a still and nonsublimated substrate to produce a thin, dense coating [15]. This sublimation mechanism resulted in the formation of a porous poly-*p*-xylylene monolith [16,17]. Such a unique fabrication process, with the use of doped ice templates, has also been exploited to fabricate tissue repair membranes [18] and scaffolds for stem cell cultures [19]; however, only composites combined with other functional materials have been used for these works in the past. On the other hand, the functionalization of the poly-*p*-xylylene polymers can be prepared by modifying the substituents of [2,2]paracyclophane precursors, and a variety of such substitutions have been produced for functionalized poly-*p*-xylylene polymer and copolymer coatings and applications [20–32]. Therefore, in the current work, we hypothesized that maleimide-substituted [2,2]paracyclophane could be used during vapor sublimation on an iced substrate, and that vapor deposition by such a precursor can produce a maleimide-functionalized poly-*p*-xylylene in porous and monolith forms (Figure 1). Compared to the maleimide-functionalized coating prepared previously [33], the current monolith poly-*p*-xylylene comprised (i) porous and structural information in three dimensions and (ii) a maleimide functionality that exhibits specific reactivity toward thiol-terminated biomolecules. This unique fabrication process, and the resultant polymer product, combines interface properties from its surface porosity, topology, and specific chemical reactivity and provides a robust tool with enhanced synergistic ability for biointerface engineering.

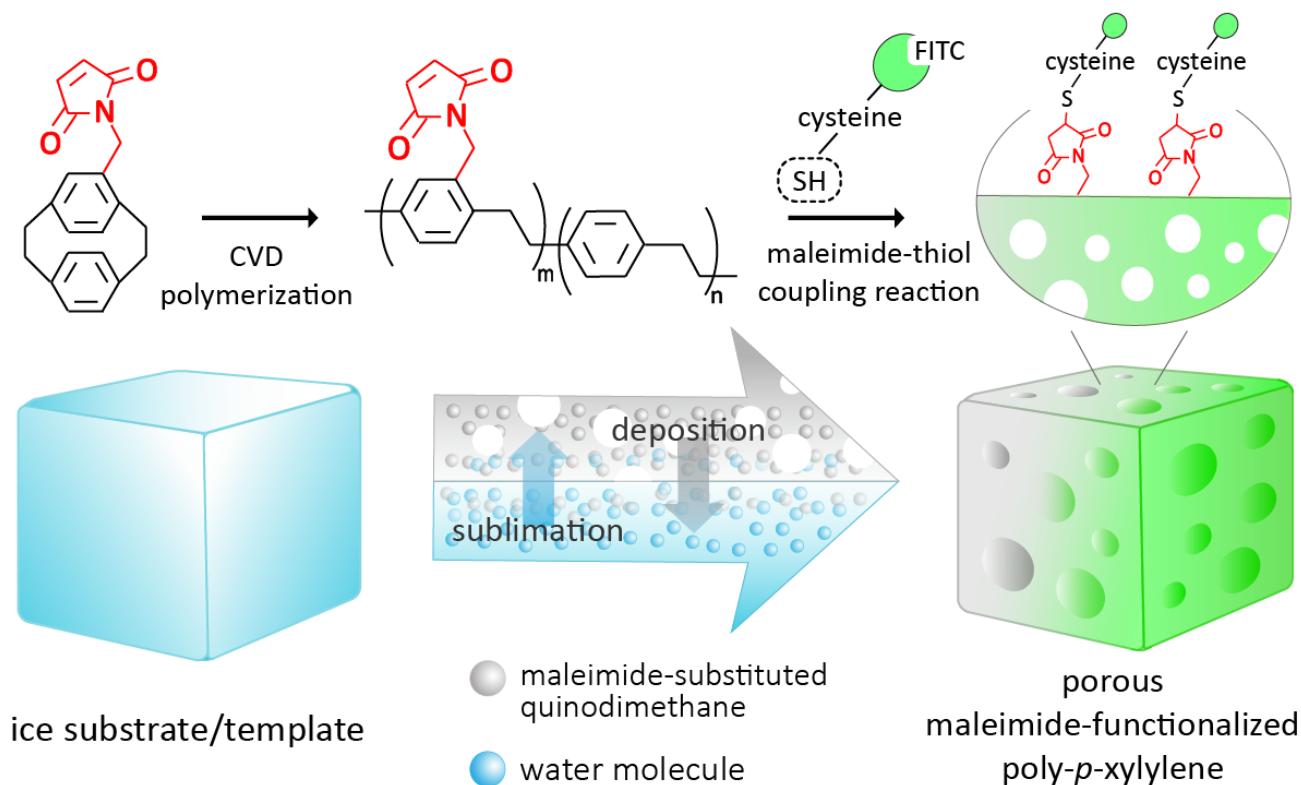


Figure 1. A schematic illustration of vapor-phase fabrication by chemical vapor deposition polymerization of 4-N-maleimidomethyl-[2,2]paracyclophane on a sublimating ice substrate/template to construct a porous and maleimide-functionalized poly-*p*-xylylene material. The resultant functional material exhibits interface chemical properties and is readily able to perform the maleimide-thiol click reaction under mild conditions.

2. Materials and Methods

2.1. Fabrication Process

For the production of poly-*p*-xylylene three-dimensional porous materials, cube-shaped ice templates, with the dimensions of $300 \mu\text{m} \times 300 \mu\text{m} \times 300 \mu\text{m}$, were prepared in order to prove the concept of the reported fabrication process. Using a negative mold of polydimethylsiloxane (PDMS) with the same dimensions to prepare this ice template, it was created as previously reported for the PDMS mold [34]. For the preparation of the ice templates, deionized water was held in the PDMS mold, and then the solution underwent a solidification process using a liquid nitrogen bath to transform the water into ice, which was then retrieved from the PDMS mold after a few minutes to obtain the ice templates. The obtained ice templates were then used for further vapor sublimation and deposition processes. During the vapor deposition, 4-N-maleimidomethyl-[2,2]paracyclophane was used as the starting material, and the monomer was polymerized and deposited to form poly[(4-N-maleimidomethyl-*p*-xylylene)-co-(*p*-xylylene)] via chemical vapor deposition (CVD) polymerization. The starting materials were vaporized under reduced pressure at 100 mTorr and approximately 90°C , followed by pyrolysis at approximately 670°C , for conversion to highly reactive monomers. During the vapor sublimation, the prepared ice templates were placed in the chamber with an operating environment of approximately 4°C and 100 mTorr, which is below the triple point for ice. From a thermodynamic point of view, ice naturally undergoes a sublimation process from the solid phase to the vapor phase. Under the same conditions, the vapor-phase monomer of the maleimide-functionalized poly-*p*-xylylene underwent polymerization and was then simultaneously deposited onto the ice surface. During the above fabrication process, argon gas, with a mass flow rate of 20 sccm (standard cubic centimeter per minute), was used as a carrier gas for transporting the starting material for the sublimation of the maleimide-substituted [2,2]paracyclophane.

Depending on the feed amount of the starting material, the deposition rate was adjusted to approximately 0.5 to 1.0 Å/s and monitored by a real-time quartz crystal microbalance (QCM) sensor (STM-100/MF, East Syracuse, NY, USA) mounted in the deposition chamber.

2.2. Characterizations

Ice substrate/template images were recorded by using a cryo-SEM (scanning electron microscope) instrument (Tabletop TM-3000, Hitachi, Tokyo, Japan), and the samples were examined at the sample stage by cooling with a continuous supply of liquid nitrogen. SEM was performed with an electron energy of 15 keV and a pressure of 100 mTorr. The detection of poly-*p*-xylylene bulks was performed with a Nova NanoSEM 230 scanning electron microscope (FEI, Hillsboro, OR, USA) that was operated at room temperature under a reduced pressure of 4×10^{-6} Torr. A micro-CT (micro computed tomography) X-ray imaging system (SkyScan 1176, Bruker, Billerica, MA, USA) was used to examine the three-dimensional images of the porous structures that scanned the sample at 40 kV. The scanning resolution was 9 μm voxels with an integration time of 2000 ms per projection. The acquired projection images were converted into three dimensional (3D) images using CTvox software (Bruker, Billerica, MA, USA). The FTIR spectra were recorded with a Spectrum 100 FTIR spectrometer (PerkinElmer, Waltham, MA, USA). During spectral acquisition, a liquid nitrogen-cooled mercury–cadmium–telluride (MCT) detector and an advanced grazing angle specular reflectance accessory (PIKE Technologies, Fitchburg, WI, USA) were applied. The scanning range was from 500 cm^{-1} to 4000 cm^{-1} with 64 acquisitions each time. The X-ray photoelectron spectroscopy (XPS) was completed using monochromatic Al K-alpha radiation as the X-ray source with 150 kW of power. The process was performed with a Theta Probe X-ray photoelectron spectrometer (Thermo Scientific, Leicestershire, UK). Elemental analysis of high-resolution C1s was performed at a flux energy level of 20 eV, and the experimental results were compared with the theoretical (calculated) values based on the proposed chemical structures. Analysis of the real-time mass spectra was carried out with a residual gas analyzer (RGA, Hiden Analytical, Warrington, UK) mounted on the deposition chamber. The RGA was operated at 10^{-9} Torr in an ultrahigh vacuum with an ionizing emission current of 20 μA and ionizing electron energy of 70 eV. The fluorescence images were obtained with a TCS SP5 CLSM confocal laser-scanning microscope (Leica Microsystems, Wetzlar, Germany) with an Ar/ArKr laser light source (wavelength: 488 nm) to detect the fluorescein (FITC)-labeled cysteine (emission wavelength: 505–525 nm).

2.3. Conjugations

The conjugation of FITC-labeled cysteine (Thermo Fisher Scientific, Waltham, MA, USA) was carried out by the reaction of a 5 mM molecular solution of FITC-labeled cysteine with the thiol groups of a manufactured sample of porous material for 4 h at 20 °C. To remove excess and unreacted reagents from the conjugated samples, a washing process was performed using the following procedure: wash three times with phosphate buffered saline (PBS, pH = 7.4, containing Tween 20, Sigma-Aldrich, St. Louis, MO, USA), once with PBS (without Tween 20) and finally rinse with deionized water.

3. Results and Discussion

To fabricate the proposed maleimide-functionalized poly-*p*-xylylene materials, ice templates were first constructed, and a reported mechanism showed that the vapor deposition of polychloro-*p*-xylylene on a dynamic substrate of the sublimating ice can result in a final porous and three-dimensional polychloro-*p*-xylylene material [17]. Theoretically, other poly-*p*-xylylene systems, such as its functionalized derivatives [15] and the maleimide-functionalized poly-*p*-xylylene proposed herein, which have been deposited using the same conventional chemical vapor deposition (CVD) polymerization, should be extendable and applied on an ice substrate. Thus, in this experiment, the preparation of the ice substrates/templates was enabled by using a polydimethylsiloxane (PDMS) mold, with the dimensions of $300 \mu\text{m} \times 300 \mu\text{m} \times 300 \mu\text{m}$, and resulted in ice cubes

with the same dimensions, analogous to how ice cubes are made. For vapor deposition, a maleimide-substituted [2,2]paracyclophane starting material was synthesized via the reported routes [33]; theoretically, in the conventional CVD polymerization, these starting materials were sublimated at approximately 90 °C under a reduced pressure of 100 mTorr and pyrolyzed at 540 °C, forming highly reactive monomer quinodimethanes species. Finally, these monomers underwent radical polymerization upon condensation at a low temperature (40 °C or below) and solid substrate formation of thin-film coatings [27,33,35]. However, in the experiments herein, the vapor deposition and polymerization occurred on the prepared ice substrates/templates and under the devised thermodynamic conditions (10 °C and under 100 mTorr). The ice substrate transformed from its solid phase to a vapor phase by sublimation, and the deposition and polymerization of quinodimethane occurred on the dynamic ice substrate instead of a conventional solid substrate. The vapor composition during the process was measured by a mass spectrometric residual gas analyzer (RGA). The recorded mass spectra in Figure 2 indicated the presence of sublimating H₂O molecules at 18 amu, the Ar carrier gas at 40 amu, and pyrolyzed quinodimethane monomers and derivatives, including N-ethylmaleimide and maleimide-substituted quinodimethane, at 104 amu, 125 amu, and 213 amu, respectively. These data support the hypothesis that the proposed vapor-phase species existed and underwent the sublimation and deposition processes at the substrate interface. The two processes finally resulted in a construction mechanism [16,17] to build a porous, three-dimensional, maleimide-functionalized poly-*p*-xylylene material. As shown in Figure 3a, the scanning electron microscopy (SEM) images revealed that the resultant porous materials represented replica structures as ice substrates/templates with the same measured dimensions (300 μm × 300 μm × 300 μm). Moreover, the formed porous structures were measured to be in the range of 3 μm to 45 μm, which was confirmed with an average of 20 μm based on micro-computed tomography (micro-CT) analysis (Figure 3b). In addition, the expected interconnection of the pores due to the voids of vapor sublimation and the nucleated polymerization of the poly-*p*-xylylene was confirmed by the reconstructed micro-CT scanning images in Figure 3b, and a video is also included in the Supplementary Materials. From the pore distribution data, the total porosity was 53.8%, of which open porosity accounts for the majority (99.8%). There is an advantage to this structure when combining cell therapy or drug delivery. This structure is beneficial for cell growth, as open pores will not stop drugs from moving, and the drug can also be released smoothly to work in the open pore. Moreover, with closed pores, the materials will be blocked from the outside. However, closed pores only account for 0.2% of the total pores. Various types of porosity and pore sizes were computed during the micro-CT analysis (Figure 3c). Hence, in this study, we demonstrate that micro-CT is versatile in evaluating scaffolds and is able to characterize them from multiple aspects.

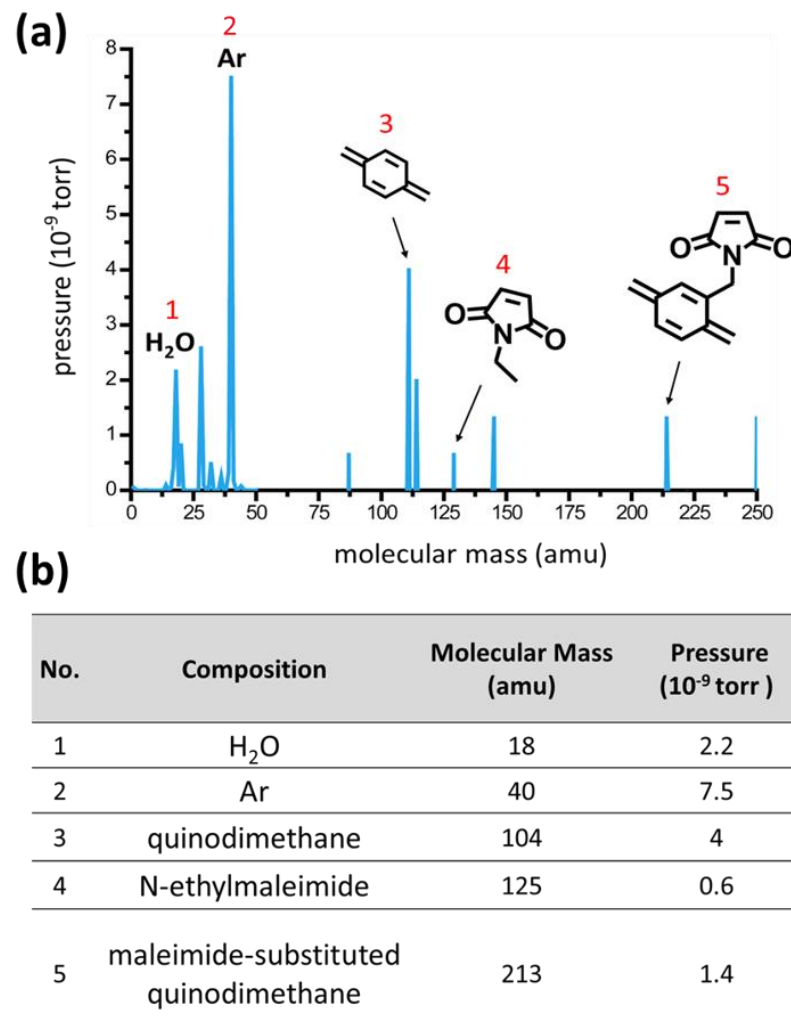


Figure 2. The characterizations of the vapor compositions, based on mass spectrometric analysis using a (residual gas analyzer) RGA during the fabrication process. The recorded mass spectra in (a) show the presence of 5 expected molecules: (1) the sublimating water molecules at 18 amu, (2) the carrier gas of argon at 40 amu, (3) the depositing quinodimethane at 104 amu, (4) a fraction of N-ethylmaleimide at 125 amu, and (5) the maleimide-substituted quinodimethane at 213 amu. (b) A table summarizing the details of the detected molecules in the vapor compositions.

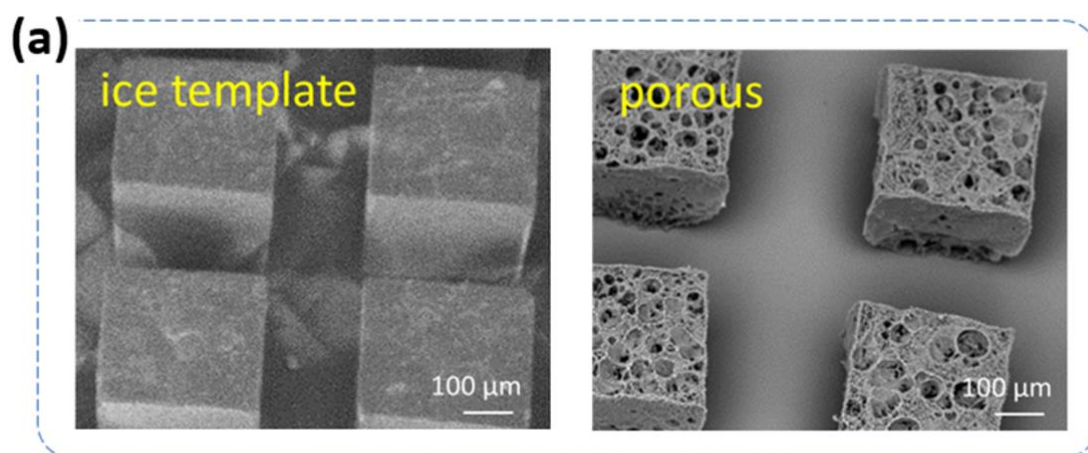


Figure 3. Cont.

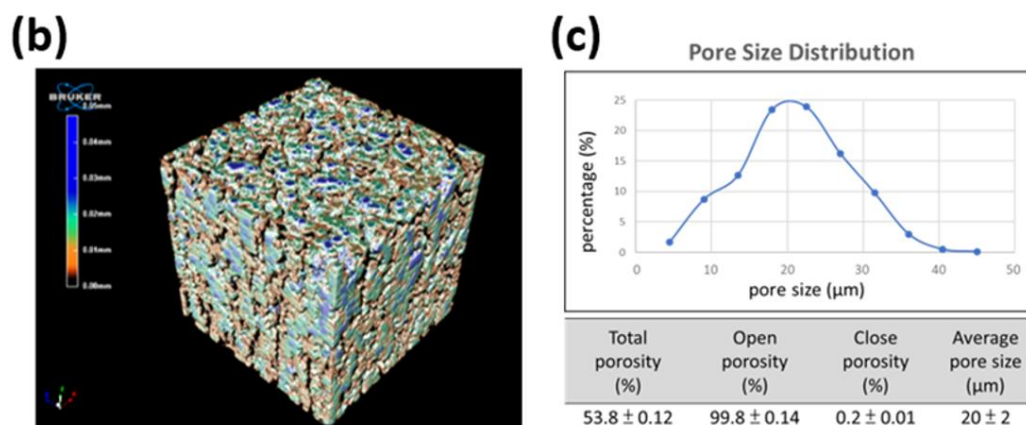


Figure 3. The characterization of the porous structures and porosity. (a) Scanning electron microscopy (SEM) images showed that cube-shaped ice templates, with the dimensions of $300\ \mu\text{m} \times 300\ \mu\text{m} \times 300\ \mu\text{m}$, were used to form porous maleimide-functionalized poly-*p*-xylylene materials by the proposed fabrication method. (b) A reconstructed micro-CT image shows the three-dimensional structure and the pore structures. (c) The calculated pore size distribution based on a micro-CT analysis suggests an interconnected pore structure (high open porosity) with an average porosity of $53.8 \pm 0.12\%$ and an average pore size of $20 \pm 2\ \mu\text{m}$.

Furthermore, the chemical structures of the resulting porous materials were verified by using Fourier transform infrared (FT-IR) spectroscopy, X-ray photoelectron spectroscopy (XPS), and mass spectrometry analysis. As shown in Figure 4, the FT-IR spectra compared the characteristic peaks of the porous materials of the maleimide-functionalized poly-*p*-xylylene with the thin-film form of this polymer that was deposited on a conventional, gold-coated silicon wafer solid substrate. The verification of the maleimide functionality was found from the peaks between 1704 to $1775\ \text{cm}^{-1}$ that were attributed to C=O bands, while the peak at $1345\ \text{cm}^{-1}$ was from the C-N bond of maleimide. Additionally, the characteristic peaks widely seen for poly-*p*-xylylenes and their derivatives were also observed from 2920 to $2854\ \text{cm}^{-1}$ [26,27,30,32,33,36]. Compared to the pure poly-*p*-xylylene, the spectra of the maleimide-functionalized poly-*p*-xylylene were found to be significantly higher with the peaks of C=O and C-N bonds. In addition, the comparison with pure (non-functionalized) poly-*p*-xylylene spectra showed an absence of C=O and C-N bonds for the pure poly-*p*-xylylene, and strong aromatic C=C bands (1530 to $1480\ \text{cm}^{-1}$) were discovered for the pure poly-*p*-xylylene but weak bands were discovered for the maleimide-functionalized poly-*p*-xylylene groups. The variations in the aromatic C=C bands, and in other fingerprint regions for different poly-*p*-xylylene derivatives, were also previously reported [30,33,37,38]. On the other hand, XPS analyses confirmed the molecular compositions and chemical structures. As shown in the XPS high-resolution C_{1s} spectrum (Figure 5), the signal at $285.0\ \text{eV}$ belonged to the aliphatic and aromatic carbons (C-C, C-H). In addition, the $76.7\ \text{atom}\%$ intensity was consistent with the theoretical concentration of $76.2\ \text{atom}\%$, and the anticipated binding states, including C-C=O, C-N, O=C-N, and $\pi \rightarrow \pi^*$ transition bonds (indicated in the enlarged image), were also analyzed. The characteristic signals at $286.0\ \text{eV}$ and $286.7\ \text{eV}$, whose calculated values were $9.6\ \text{atom}\%$ and $4.6\ \text{atom}\%$, respectively, corresponded to the C-C=O and C-N bonds matching the theoretical values of $9.5\ \text{atom}\%$ and $4.8\ \text{atom}\%$, respectively. The signal at $289.2\ \text{eV}$ had a comparably low value from O=C-N bonds ($6.7\ \text{atom}\%$ compared to the theoretical value of $9.5\ \text{atom}\%$), and the signal at $291.5\ \text{eV}$ ($2.4\ \text{atom}\%$) indicated $\pi \rightarrow \pi^*$ transitions that are characteristic of aromatic polymers and have been reported for other functionalized poly-*p*-xylylenes [38]. Collectively, the combined FT-IR and XPS data confirm the chemical structures and support the assumption of the synthesized porous maleimide-functionalized poly-*p*-xylylene materials.

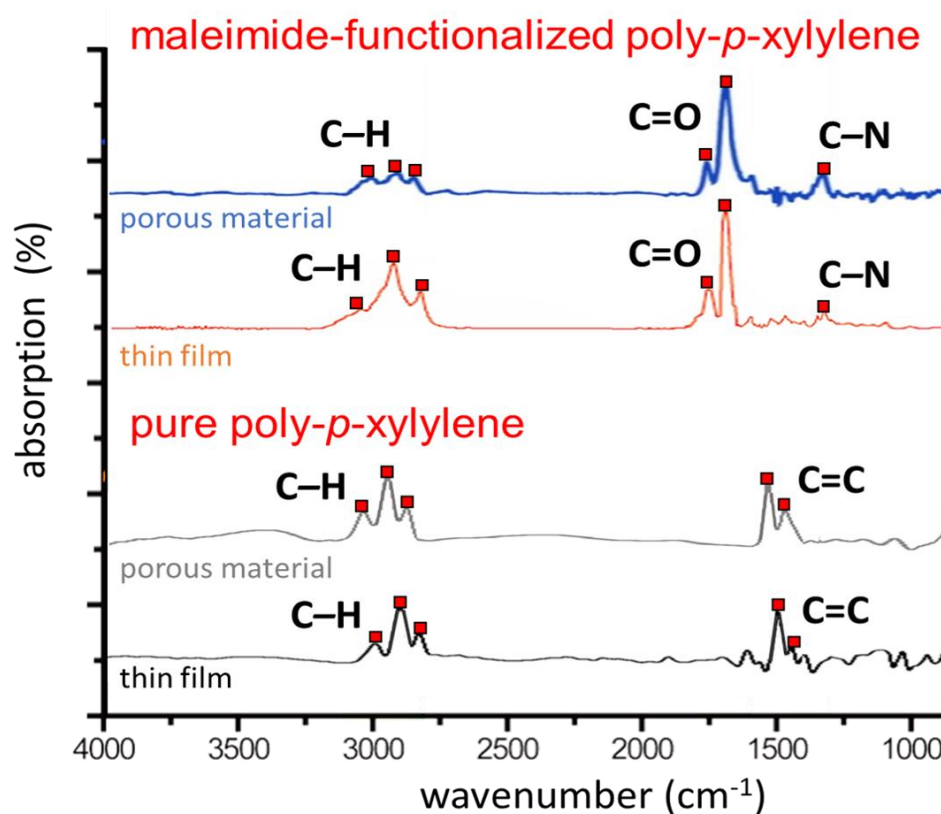


Figure 4. Fourier transform infrared (FT-IR) analysis showed consistent spectra. Characteristic peaks of the maleimide-functionalized poly-*p*-xylylene were detected for C-H, C=O, and C-N on the fabricated porous materials. The results were compared to a thin-film maleimide-functionalized poly-*p*-xylylene and pure (non-functionalized) poly-*p*-xylylenes.

To further verify the maleimide functionality of the fabricated 3D porous materials that would be available to perform bio-orthogonal reactions toward thiol-terminated molecules, we devised a series of conjugation experiments for the fabricated samples. The maleimide functionality enabled a Michael-type addition that crossed the unsaturated carbon-carbon bonds of the maleimide moiety and specifically reacted with a thiol group. The reaction represented a class of mild, but specific, reactions that were able to conjugate thiol-terminated molecules (widely available in biological systems) at room temperature and in water solvents without the need for metal catalysts, a high temperature, or UV irradiation. Analogous to a series of click reactions, including thiol-ene or thiol-yne reactions and azide-alkyne 1,3-dipolar cycloaddition, the maleimide-thiol coupling reaction has also been described due to its click characteristics and benign reaction conditions [39]. In these experiments, fluorescein (FITC)-labeled cysteines were selected as a model molecule for demonstration, and via the aforementioned reaction mechanism, maleimide specifically clicked to the thiol terminus of a cysteine residue (i.e., the distributed maleimide functionality at the material interface readily reacted with cysteine-FITC, and green-channelled FITC fluorescence signals were therefore detected in the expected and registered areas). As indicated in Figure 6, the FITC signals detected by the confocal laser scanning microscopy (CLSM) showed the same $300\ \mu\text{m} \times 300\ \mu\text{m} \times 300\ \mu\text{m}$ array patterns that were consistent in both the ice substrates/templates and the fabricated maleimide-functionalized poly-*p*-xylylene porous materials. The coupling reaction ensured firm covalent bonding between the maleimide and thiol, and precise interface chemistry could be realized compared to approaches using physical adsorption and desorption, which comprise loosely bound interactions that are usually uncontrollable [40]. Therefore, in control experiments, a nonfunctionalized poly-*p*-xylylene porous material was fabricated from unsubstituted [2,2]paracyclophane, and the same ice substrates/templates were used to attempt the

same conjugation reaction by applying cysteine-FITC molecules to the fabricated samples. However, due to the lack of the required maleimide functionality, only the physically and loosely bound cysteine-FITC molecules were attached to the sample surfaces; a regular wash process with detergent removed these physically adsorbed molecules from the samples, and only suppressed fluorescence signals were detected [25,30]. In addition, the CLSM images were collected along the z-axis with a devised distance interval ($Z=10\ \mu\text{m}$, $50\ \mu\text{m}$, $90\ \mu\text{m}$, $130\ \mu\text{m}$, $170\ \mu\text{m}$, $210\ \mu\text{m}$, $250\ \mu\text{m}$, and $290\ \mu\text{m}$). These images, in the specific positions shown in Figure 6, indicated distinct patterns of the attached fluorescence signals and are believed to be due to conjugation occurring on the anisotropic porous structure of a maleimide-functionalized poly-*p*-xylylene within the material's 3D architecture. The sustained intensity of the fluorescence signals after the wash process also confirmed the firm attachment of cysteine-FITC via the conjugation reaction. The fabricated maleimide-functionalized poly-*p*-xylylene materials provided a porous structure and additionally exhibited clickable functional conduct from the maleimide available on the material interface for specific targeting of thiol-terminated molecules, which are widely seen in biological systems. Such porous and functional products are expected to have unlimited applicability.

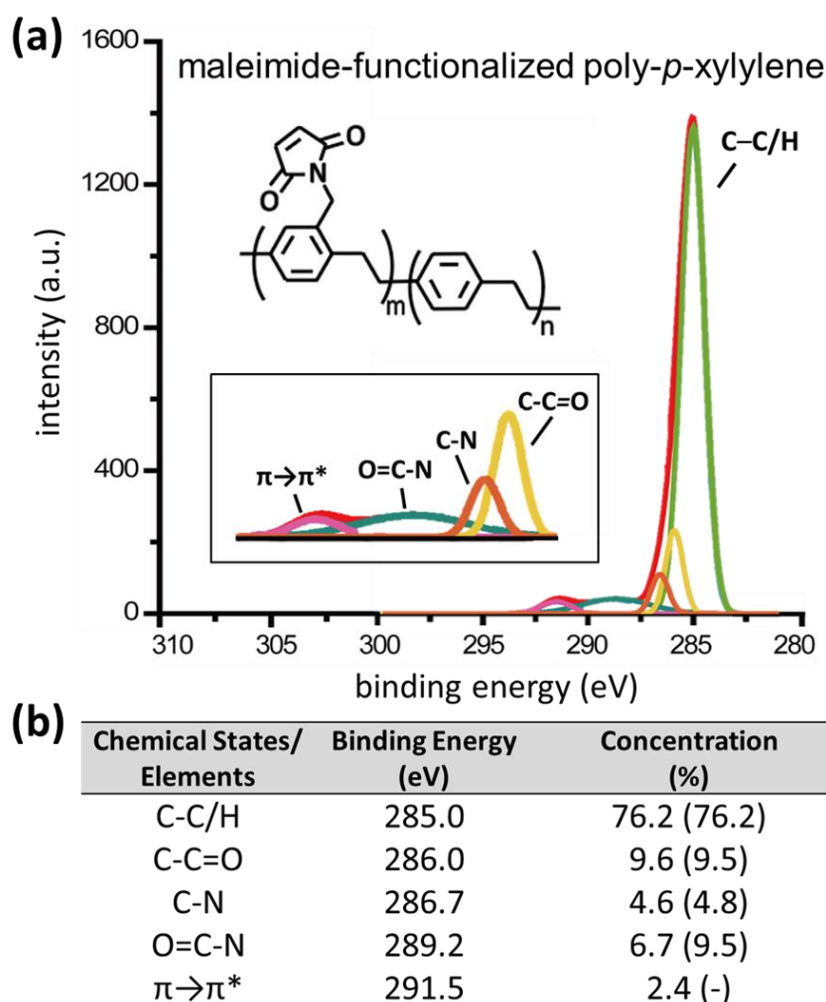


Figure 5. (a) X-ray photoelectron spectroscopy (XPS) high-resolution analysis shows the recorded spectra of the fabricated porous maleimide-functionalized poly-*p*-xylylene. Details of the deconvolution spectra showing components with respect to a specific binding energy, including C-C=O, C-N, O=C-N, and $\pi\rightarrow\pi^*$ transition bonds, are indicated in the enlarged image. (b) Detailed chemical compositions were confirmed by comparing the binding energies of the expected chemical states for the experimental values with the theoretical values (in brackets).

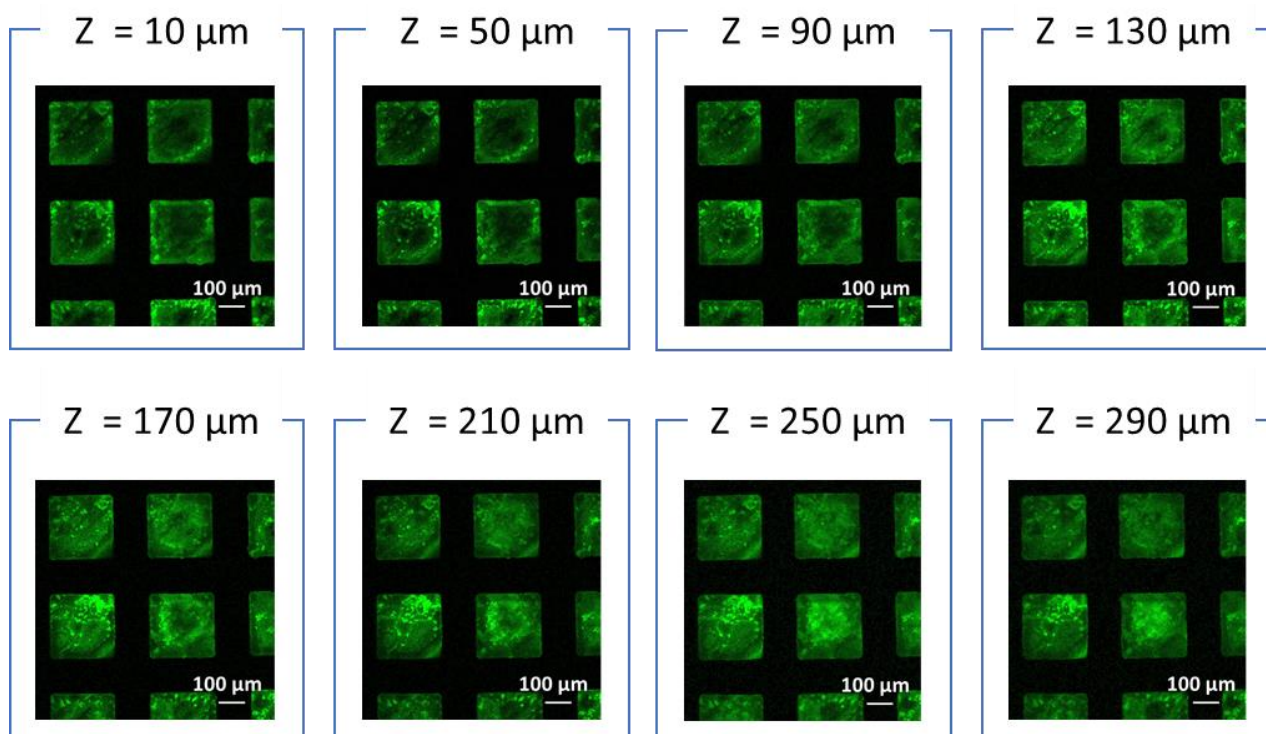


Figure 6. An analysis of the reactivity of the fabricated porous maleimide-functionalized poly-*p*-xylylenes. The fluorescence images recorded by confocal laser scanning microscopy (CLSM) showed consistent $300\ \mu\text{m} \times 300\ \mu\text{m}$ arrayed patterns that confirmed the conjugation between the fluorescein (FITC)-labeled cysteine and the maleimide group on the porous materials, and the images at various Z-axes (with a $40\ \mu\text{m}$ spacing interval from $10\ \mu\text{m}$ to $290\ \mu\text{m}$) further verified the reactivity on the interface of the porous materials in three dimensions.

4. Conclusions

A unique fabrication process by vapor sublimation and vapor deposition to produce a porous and functionalized poly-*p*-xylylene monolith material was introduced in the current work. The monolith comprised structural information in terms of porosity and topology and, more importantly, a maleimide functional moiety for specific conjugation reactivity via a maleimide–thiol coupling reaction. The vapor-phase fabrication process was simple, clean, and free of harsh chemical agents, and the poly-*p*-xylylene used is a USP (United States Pharmacopoeia) Class VI biocompatible material, which is favorable for sensitive applications. The enhanced and synergistic interface properties, combining the porosity and chemical functionality of the fabricated porous monolith, represent robust bioengineering materials and will be useful for unlimited applications in scaffolding for tissue engineering, biosensors, bioimaging, targeted drug-eluting devices, and regenerative materials.

Supplementary Materials: The following are available online at <https://www.mdpi.com/article/10.3390/coatings11040466/s1>, Video S1: Reconstruction images of the three-dimensional pore structure by micro-CT.

Author Contributions: Conceptualization, S.-M.H., C.-Y.L., Y.-C.Y., Y.-C.C. and H.-Y.C.; methodology, S.-M.H., C.-Y.L., Y.-C.Y. and H.-Y.C.; precursor synthesis, T.K., T.-Y.W., N.-Y.C., J.C., Y.-R.C.; CVD polymerization and characterizations, S.-M.H., C.-Y.L., T.-Y.W., Y.-R.C.; micro-CT software analysis, J.-Q.X., and Y.-M.C.; validation, S.-M.H., C.-Y.L., T.K. and T.-Y.W.; fluorescence visualization and analysis, C.-Y.L. and C.-W.H.; XPS analysis, S.-M.H., J.C., Y.-R.C. and Y.-R.C.; FT-IR analysis S.-M.H., C.-Y.L., Y.-R.C. and Y.-R.C.; data curation, S.-M.H., C.-Y.L., Y.-M.C. and Y.-R.C.; writing—original draft preparation, S.-M.H., C.-Y.L., Y.-C.Y. and H.-Y.C.; writing—review and editing, S.-M.H., C.-Y.L., Y.-C.C. and H.-Y.C.; supervision, Y.-C.Y., Y.-C.C. and H.-Y.C.; project administration, Y.-C.Y., Y.-C.C. and H.-Y.C.; funding acquisition, Y.-C.C. and H.-Y.C. All authors have read and agreed to the published version of the manuscript.

Funding: This research was funded by the Ministry of Science and Technology of Taiwan (MOST 108-2221-E-002-169-MY3; 108-2218-E-007-045; 109-2314-B-002-041-MY3; 109-2634-F-002-042). In addition, this work was further supported by the “Advanced Research Center for Green Materials Science and Technology” from The Featured Area Research Center Program within the framework of the Higher Education Sprout Project by the Ministry of Education (109L9006).

Institutional Review Board Statement: Not applicable.

Informed Consent Statement: Not applicable.

Data Availability Statement: All data generated or analyzed during this study are included in this published article and its supplementary information files.

Conflicts of Interest: The authors declare no conflict of interest. The funders had no role in the design of the study; in the collection, analyses, or interpretation of data; in the writing of the manuscript, or in the decision to publish the results.

References

1. Chai, G.S.; Yoon, S.B.; Yu, J.-S.; Choi, J.-H.; Sung, Y.-E. Ordered Porous Carbons with Tunable Pore Sizes as Catalyst Supports in Direct Methanol Fuel Cell. *J. Phys. Chem. B* **2004**, *108*, 7074–7079. [[CrossRef](#)]
2. Kosuge, K.; Kubo, S.; Kikukawa, N.; Takemori, M. Effect of Pore Structure in Mesoporous Silicas on VOC Dynamic Adsorption/Desorption Performance. *Langmuir* **2007**, *23*, 3095–3102. [[CrossRef](#)]
3. Li, Y.Y.; Cunin, F.; Link, J.R.; Gao, T.; Betts, R.E.; Reiver, S.H.; Chin, V.; Bhatia, S.N.; Sailor, M.J. Polymer Replicas of Photonic Porous Silicon for Sensing and Drug Delivery Applications. *Science* **2003**, *299*, 2045–2047. [[CrossRef](#)] [[PubMed](#)]
4. Wales, D.J.; Grand, J.; Ting, V.P.; Burke, R.D.; Edler, K.J.; Bowen, C.R.; Mintova, S.; Burrows, A.D. Gas Sensing Using Porous Materials for Automotive Applications. *Chem. Soc. Rev.* **2015**, *44*, 4290–4321. [[CrossRef](#)]
5. Horcajada, P.; Chalati, T.; Serre, C.; Gillet, B.; Sebrie, C.; Baati, T.; Eubank, J.F.; Heurtaux, D.; Clayette, P.; Kreuz, C. Porous Metal–Organic–Framework Nanoscale Carriers as a Potential Platform for Drug Delivery and Imaging. *Nat. Mater.* **2010**, *9*, 172–178. [[CrossRef](#)]
6. Santos, H.A.; Mäkilä, E.; Airaksinen, A.J.; Bimbo, L.M.; Hirvonen, J. Porous Silicon Nanoparticles for Nanomedicine: Preparation and Biomedical Applications. *Nanomedicine* **2014**, *9*, 535–554. [[CrossRef](#)] [[PubMed](#)]
7. Zhang, Y.; Yang, L.; Yan, L.; Wang, G.; Liu, A. Recent Advances in the Synthesis of Spherical and Nanomof-Derived Multifunctional Porous Carbon for Nanomedicine Applications. *Coord. Chem. Rev.* **2019**, *391*, 69–89. [[CrossRef](#)]
8. Pounder, R.J.; Stanford, M.J.; Brooks, P.; Richards, S.P.; Dove, A.P. Metal Free Thiol–Maleimide ‘Click’ Reaction as a Mild Functionalisation Strategy for Degradable Polymers. *Chem. Commun.* **2008**, 5158–5160. [[CrossRef](#)] [[PubMed](#)]
9. Tron, G.C.; Pirali, T.; Billington, R.A.; Canonico, P.L.; Sorba, G.; Genazzani, A.A. Click Chemistry Reactions in Medicinal Chemistry: Applications of the 1, 3-dipolar Cycloaddition Between Azides and Alkynes. *Med. Res. Rev.* **2008**, *28*, 278–308. [[CrossRef](#)]
10. Blackman, M.L.; Royzen, M.; Fox, J.M. Tetrazine Ligation: Fast Bioconjugation Based on Inverse-Electron-Demand Diels–Alder Reactivity. *J. Am. Chem. Soc.* **2008**, *130*, 13518–13519. [[CrossRef](#)]
11. Best, M.D. Click Chemistry and Bioorthogonal Reactions: Unprecedented Selectivity in the Labeling of Biological Molecules. *Biochemistry* **2009**, *48*, 6571–6584. [[CrossRef](#)]
12. Ciampi, S.; Böcking, T.; Kilian, K.A.; Harper, J.B.; Gooding, J.J. Click Chemistry in Mesoporous Materials: Functionalization of Porous Silicon Rugate Filters. *Langmuir* **2008**, *24*, 5888–5892. [[CrossRef](#)] [[PubMed](#)]
13. Xi, W.; Scott, T.F.; Kloxin, C.J.; Bowman, C.N. Click Chemistry in Materials Science. *Adv. Funct. Mater.* **2014**, *24*, 2572–2590. [[CrossRef](#)]
14. L’abbé, G. Decomposition and Addition Reactions of Organic Azides. *Chem. Rev.* **1969**, *69*, 345–363. [[CrossRef](#)]
15. Chen, H.-Y.; Lahann, J. Designable Biointerfaces Using Vapor-Based Reactive Polymers. *Langmuir* **2010**, *27*, 34–48. [[CrossRef](#)]
16. Tung, H.-Y.; Guan, Z.-Y.; Liu, T.-Y.; Chen, H.-Y. Vapor Sublimation and Deposition to Build Porous Particles and Composites. *Nat. Commun.* **2018**, *9*, 2564. [[CrossRef](#)]
17. Tung, H.-Y.; Sun, T.-P.; Sun, H.-Y.; Guan, Z.-Y.; Hu, S.-K.; Chao, L.; Chen, H.-Y. Construction and Control of 3D Porous Structure Based on Vapor Deposition on Sublimation Solids. *Appl. Mater. Today* **2017**, *7*, 77–81. [[CrossRef](#)]
18. Lin, C.-W.; Guan, Z.-Y.; Lu, M.; Wu, T.-Y.; Cheng, N.-C.; Chen, H.-Y.; Yu, J. Synergistically Enhanced Wound Healing of a Vapor-Constructed Porous Scaffold. *ACS Appl. Bio Mater.* **2020**, *3*, 5678–5686. [[CrossRef](#)]
19. Wu, C.-Y.; Guo, C.-L.; Yang, Y.-C.; Huang, C.-W.; Zeng, J.-Y.; Guan, Z.-Y.; Chiang, Y.-C.; Wang, P.-Y.; Chen, H.-Y. Parylene-Based Porous Scaffold with Functionalized Encapsulation of Platelet-Rich Plasma and Living Stem Cells for Tissue Engineering Applications. *ACS Appl. Bio Mater.* **2020**, *3*, 7193–7201. [[CrossRef](#)]
20. Wu, C.-Y.; Liu, H.-Y.; Huang, C.-W.; Yeh, S.-Y.; Cheng, N.-C.; Ding, S.-T.; Chen, H.-Y. Synergistically Controlled Stemness and Multilineage Differentiation Capacity of Stem Cells on Multifunctional Biointerfaces. *Adv. Mater. Interfaces* **2017**. [[CrossRef](#)]
21. Wu, C.-Y.; Chang, C.-W.; Yuan, R.-H.; Chiang, Y.-C.; Chen, J.-T.; Kang, D.-Y.; Chen, H.-Y. Multifunctional Nanoparticles with Controllable Dimensions and Tripled Orthogonal Reactivity. *Nanoscale* **2017**, *9*, 14787–14791. [[CrossRef](#)]
22. Guan, Z.-Y.; Wu, C.-Y.; Chen, H.-Y. Stepwise and Programmable Cell Differentiation Pathways of Controlled Functional Biointerfaces. *Acs Biomater. Sci. Eng.* **2017**, *3*, 1815–1821. [[CrossRef](#)]

23. Chen, H.-Y. Micro- and Nano-Surface Structures Based on Vapor-Deposited Polymers. *Beilstein J. Nanotechnol.* **2017**, *8*, 1366–1374. [[CrossRef](#)] [[PubMed](#)]
24. Wu, C.-Y.; Huang, C.-W.; Guan, Z.-Y.; Wu, J.-T.; Yeh, S.-Y.; Su, C.-T.; Chang, C.-H.; Ding, S.-T.; Chen, H.-Y. Vapor-based Coatings for Antibacterial and Osteogenic Functionalization and the Immunological Compatibility. *Mater. Sci. Eng. C* **2016**, *69*, 283–291. [[CrossRef](#)] [[PubMed](#)]
25. Sun, T.-P.; Tai, C.-H.; Wu, J.-T.; Wu, C.-Y.; Liang, W.-C.; Chen, H.-Y. Multifaceted and Route-Controlled "Click" Reactions based on Vapor-Deposited Coatings. *Biomater. Sci.* **2016**, *4*, 265–271. [[CrossRef](#)]
26. Guan, Z.-Y.; Wu, C.-Y.; Wu, J.-T.; Tai, C.-H.; Yu, J.; Chen, H.-Y. Multifunctional and Continuous Gradients of Biointerfaces Based on Dual Reverse Click Reactions. *ACS Appl. Mater. Interfaces* **2016**, *8*, 13812–13818. [[CrossRef](#)]
27. Tsai, M.-Y.; Chen, Y.-C.; Lin, T.-J.; Hsu, Y.-C.; Lin, C.-Y.; Yuan, R.-H.; Yu, J.; Teng, M.-S.; Hirtz, M.; Chen, M.H.-C.; et al. Vapor-Based Multicomponent Coatings for Antifouling and Biofunctional Synergic Modifications. *Adv. Funct. Mater.* **2014**, *24*, 2281–2287. [[CrossRef](#)]
28. Sun, H.-Y.; Fang, C.-Y.; Lin, T.-J.; Chen, Y.-C.; Lin, C.-Y.; Ho, H.-Y.; Chen, M.H.C.; Yu, J.; Lee, D.-J.; Chang, C.-H.; et al. Thiol-Reactive Parylenes as a Robust Coating for Biomedical Materials. *Adv. Mater. Interfaces* **2014**, *1*, 1400093. [[CrossRef](#)]
29. Su, C.-T.; Yuan, R.-H.; Chen, Y.-C.; Lin, T.-J.; Chien, H.-W.; Hsieh, C.-C.; Tsai, W.-B.; Chang, C.-H.; Chen, H.-Y. A Facile Approach Toward Protein-Resistant Biointerfaces Based on Photodefinable Poly-P-Xylylene Coating. *Colloids Surf. B Biointerfaces* **2014**, *116*, 727–733. [[CrossRef](#)]
30. Chen, H.-Y.; Lin, T.-J.; Tsai, M.-Y.; Su, C.-T.; Yuan, R.-H.; Hsieh, C.-C.; Yang, Y.-J.; Hsu, C.-C.; Hsiao, H.-M.; Hsu, Y.-C. Vapor-Based Tri-Functional Coatings. *Chem. Commun.* **2013**, *49*, 4531–4533. [[CrossRef](#)]
31. Wu, M.-G.; Hsu, H.-L.; Hsiao, K.-W.; Hsieh, C.-C.; Chen, H.-Y. Vapor-Deposited Parylene Photoresist: A Multipotent Approach toward Chemically and Topographically Defined Biointerfaces. *Langmuir* **2012**, *28*, 14313–14322. [[CrossRef](#)] [[PubMed](#)]
32. Wu, J.-T.; Huang, C.-H.; Liang, W.-C.; Wu, Y.-L.; Yu, J.; Chen, H.-Y. Reactive Polymer Coatings: A General Route to Thiol-ene and Thiol-yne Click Reactions. *Macromol. Rapid Commun.* **2012**, *33*, 922–927. [[CrossRef](#)] [[PubMed](#)]
33. Tsai, M.-Y.; Lin, C.-Y.; Huang, C.-H.; Gu, J.-A.; Huang, S.-T.; Yu, J.; Chen, H.-Y. Vapor-based Synthesis of Maleimide-Functionalized Coating for Biointerface Engineering. *Chem. Commun.* **2012**, *48*, 10969–10971. [[CrossRef](#)]
34. Chen, H.-Y.; Lahann, J. Vapor-Assisted Micropatterning in Replica Structures: A Solventless Approach towards Topologically and Chemically Designable Surfaces. *Adv. Mater.* **2007**, *19*, 3801–3808. [[CrossRef](#)]
35. Tsai, Y.-T.; Wu, C.-Y.; Guan, Z.-Y.; Sun, H.-Y.; Cheng, N.-C.; Yeh, S.-Y.; Chen, H.-Y. Topologically Controlled Cell Differentiation Based on Vapor-Deposited Polymer Coatings. *Langmuir* **2017**. [[CrossRef](#)] [[PubMed](#)]
36. Guan, Z.-Y.; Wu, C.-Y.; Chen, T.-Y.; Huang, S.-T.; Chiang, Y.-C.; Chen, H.-Y. Clickable and Photo-Erasable Surface Functionalities by Using Vapor-Deposited Polymer Coatings. *ACS Biomater. Sci. Eng.* **2019**, *5*, 1753–1761. [[CrossRef](#)]
37. Chen, Y.-C.; Sun, T.-P.; Su, C.-T.; Wu, J.-T.; Lin, C.-Y.; Yu, J.; Huang, C.-W.; Chen, C.-J.; Chen, H.-Y. Sustained Immobilization of Growth Factor Proteins Based on Functionalized Parylenes. *ACS Appl. Mater. Interfaces* **2014**, *6*, 21906–21910. [[CrossRef](#)] [[PubMed](#)]
38. Lahann, J.; Langer, R. Novel Poly(p-xylylenes): Thin Films with Tailored Chemical and Optical Properties. *Macromolecules* **2002**, *35*, 4380–4386. [[CrossRef](#)]
39. Deng, X.; Friedmann, C.; Lahann, J. Bio-orthogonal "Double-Click" Chemistry Based on Multifunctional Coatings. *Angew. Chem. Int. Ed.* **2011**, *50*, 6522–6526. [[CrossRef](#)] [[PubMed](#)]
40. Guan, Z.-Y.; Huang, C.-W.; Huang, M.-C.; Wu, C.-Y.; Liu, H.-Y.; Ding, S.-T.; Chen, H.-Y. Controlling Multi-Function of Bio-materials Interfaces Based on Multiple and Competing Adsorption of Functional Proteins. *Colloids Surf. B Biointerfaces* **2017**, *149*, 130–137. [[CrossRef](#)]